CrossMark

Variations of Solar Oblateness with the 22 yr Magnetic Cycle Explain Apparently Inconsistent Measurements

Abdanour Irbah[1] , Redouane Mecheri[2], Luc Damé[1], and Djelloul Djafer[3]

[1] LATMOS/IPSL, UVSQ Université Paris-Saclay, Sorbonne Université, CNRS, 11 BD D'Alembert Guyancourt F-78280, France; air@latmos.ipsl.fr

[2] Centre de Recherche Astronomie Astrophysique et Géophysique, CRAAG Bouzaréah 16340, Algeria

[3] Unité de Recherche Appliquée en Energies Renouvelables, URAER Centre de Développement des Energies Renouvelables, CDER, Ghardaïa 47133, Algeria

Abstract

Solar oblateness results from distortion processes due to several phenomena inside of the Sun, but it can also be induced by the centrifugal potential of surface rotation. This fundamental parameter is of great scientific interest, yet for more than a century its measurements have remained a controversial topic, whether because of its average value or its variations observed (or not) over time. Special images acquired for almost the whole of Cycle 24 by the Helioseismic and Magnetic Imager on board the *Solar Dynamic Observatory* are used for calculating solar oblateness. The average oblateness obtained is 8.8 ± 0.8 mas, in good agreement with measurements over the last two decades. Variations are observed in anti-phase with the solar activity during Cycle 24, whereas they were in phase with activity during Cycle 23. More generally, the trend of both in-phase variation during odd cycles and anti-phase variation during even cycles is confirmed when revisiting past measurements. Therefore, it is possible that the Sun initiates a physical process resulting in a pulsation with the 22 yr magnetic cycle; it has extreme values during the polarity reversals, with a maximum swelling during odd cycles and the opposite for even ones. This oscillation could resolve the controversy surrounding past measurements.

*Key words:* methods: data analysis – Sun: fundamental parameters

1. Introduction

The internal dynamics of the Sun, from its depths to the most superficial layers, are manifested by visible disturbances on the surface of the photosphere, leading directly to small deviations from the sphericity of the Sun. The solar shape thus reflects the internal state of the Sun and the processes that take place there. This drew the attention of Newcomb (1865), who asked why Newtonian gravitational theory could not correctly predict the advance of Mercury's perihelion observed by Le Verrier (1859). He suggested that a 500 mas oblateness, i.e., the pole-equator radius difference due to the rapidly rotating interior of the Sun, could provide an explanation (Newcomb 1895). At that time the solar shape was understood via two main theories: the theory of gravitation and the internal rotation of the Sun. The advent of Einstein's theory of general relativity provided an explanation for the anomalous advance of Mercury's perihelion, but good estimates of solar oblateness are still a necessary element of this theory; i.e., gravitational moments of the Sun are still relevant for the Mercury perihelion (Chapman 2008).

Many measurements of solar oblateness have been carried out for several decades, generating other questions about its mean value and temporal variations. A good review of the history of oblateness measurements, and the issues that they have raised, may be found in the papers of Dicke & Goldenberg (1974) and Rozelot & Damiani (2011). Some scientific events, however, need to be revisited. The measurement of Dicke and Goldenberg's solar oblateness in 1966 in Princeton, New Jersey, is worth mentioning because of its high value (41.9 ± 3.3 mas), which allowed them to highlight the scalar-tensor theory of gravitation and the quadrupole moment of the Sun associated with a rapidly rotating core (Dicke & Goldenberg 1974). These results were widely criticized, but have sparked a growing interest in the interior of the Sun.

Among the critics, Sturrok & Gilvarry (1967) showed that a rapid change of internal magnetic field would cause magnetic distortions at the surface, resulting in an oblateness comparable to the observations. The magnetic field then appeared as the third major issue affecting the solar shape. Gravitational models with contributions from helioseismology, which probes the Sun's interior to estimate both radial profiles of latitudinal differential rotation and the internal magnetic field (Goode & Thompson 1992; Paterno et al. 1996; Antia et al. 2000), made it possible to identify acceptable values for oblateness that are mostly induced by the centrifugal force on surface layers with a very weak contribution from the gravitational quadrupole moment J_2 (Armstrong & Kuhn 1999; Mecheri et al. 2004; Antia et al. 2008). Measurements made in space (Fivian et al. 2008; Irbah et al. 2014), on balloons (Egidi et al. 2006), and on the ground (Hill & Stebbins 1975; Rozelot et al. 2009) confirmed the expected values.

Temporal variations are just as useful for understanding the functioning of the Sun in relation to its activity cycle. In particular, helioseismic inversion has revealed an insignificant temporal variation of J_2 with, in contrast, a variation in the surface layer properties (Lefebvre et al. 2007; Antia et al. 2008) correlated with the solar cycle. This suggests that variations in the shape of the Sun are certainly associated with the magnetic field. Therefore, an accurate scrutiny of the surface layers of the Sun is very important and requires high-precision helioseismology in order to provide a good resolution of their structure (Reiter et al. 2015). Time series of oblateness recorded on the ground, from balloons, and lately from space have shown variations; however, they have been inconclusive. They are in phase (Dicke et al. 1987; Emilio et al. 2007; Rozelot et al. 2009; Damiani et al. 2011) or anti-phase (Egidi et al. 2006; Meftah et al. 2016) with the solar activity, although some authors have reported no obvious variations (Kuhn et al. 2012; Figure 1). The longest time series recorded in space, which is
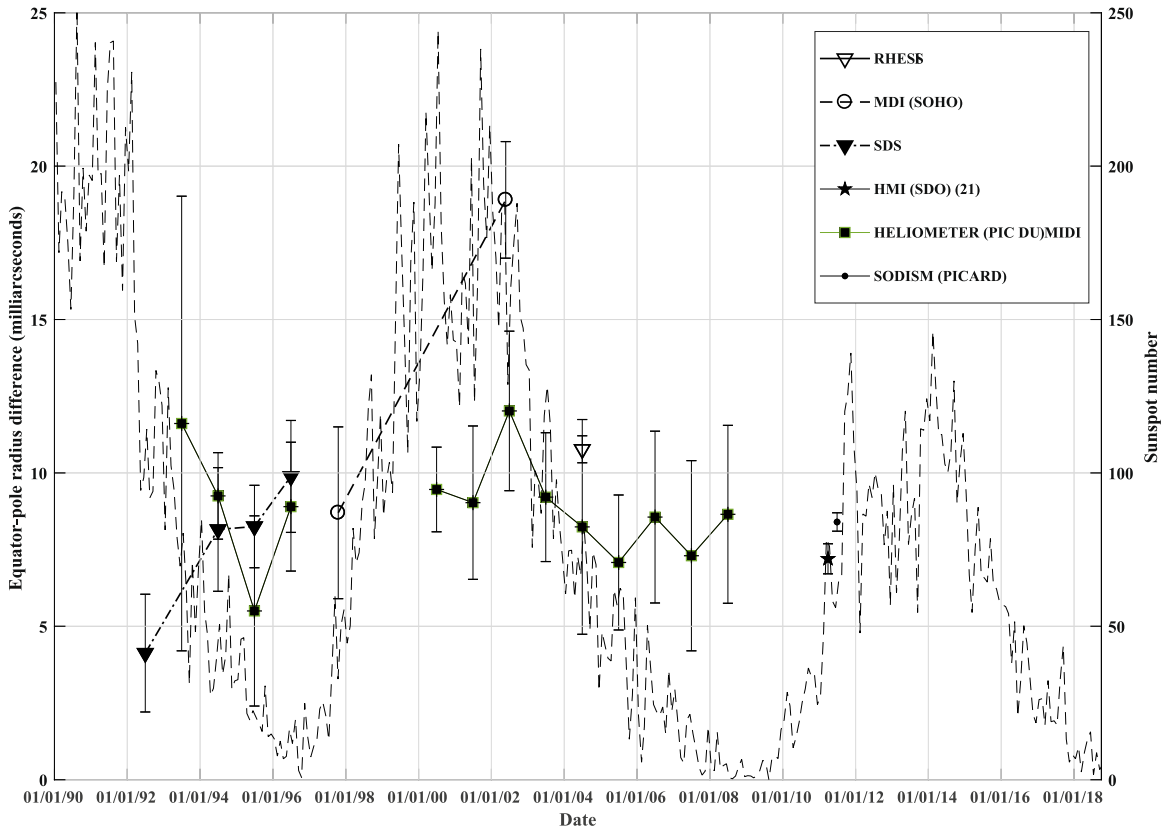
Figure 1. Equator-pole radius difference measured with the Heliometer at the *Pic du Midi* (France), with the Solar Disk Sextant (SDS) on a balloon and from space (*Reuven Ramaty High Energy Solar Spectroscopic Imager* (*RHESSI*), Michelson Doppler Imager (MDI), HMI, and the SOlar Diameter Imager and Surface Mapper (SODISM)) along with sunspot number (SILSO Data/Image 2018). The HMI value is the average over the period between 2010–2012 of previous measurements, because no variations with solar activity were reported (Kuhn et al. 2012). SDS measurements exhibit anti-phase variations in the descending phase of Cycle 22. Measurements made with the Heliometer during Cycle 22 have necessarily important error bars because they were obtained from the ground, but they still properly overlap the SDS ones. Nevertheless, their amplitudes prevent a conclusive identification of phase variation with activity. Space and ground measurements made during Cycle 23 are in phase with solar activity. Note that the first Heliometer measurement of Cycle 23, corresponding to solar activity maximum, seems underestimated. This value corresponds to the resumption of measurements with the instrument after an interruption of 2 yr (1997–1999).

still in progress, was recorded with the Helioseismic and Magnetic Imager (HMI) on board the *Solar Dynamics Observatory* (*SDO*). *SDO* was launched in 2010 February just after the beginning of Cycle 24, and the series of HMI measurements now covers almost the entire cycle. These measurements, therefore, are a major asset to being able to explain and validate those carried out in the past, including reported inconsistencies.

2. HMI Data and Processing

Angular variations of the solar shape, along with their evolution in time, are obtained from roll calibrations that have been performed on *SDO*/HMI twice a year since its launch. This calibration mode consists of rolling the spacecraft around an axis that is close to HMI's line of sight and taking images at constant angular positions during rotation (11°.25 since 2010 October). This procedure will later allow for the removal of effects on the solar shape of both mispointing and optical distortion when processing image sequences. Full images of the Sun are recorded in linear polarization at a narrow wavelength band (76 mÅ) in the solar continuum near the Fe I absorption line at 617.3 nm. They have an angular resolution of 1 arcsec. Their size and angular sampling are 4096 × 4096 pixels and 0.5 arcsec, respectively. A complete roll calibration takes about

7 hr, while the instrument is subjected to various thermal stresses on its orbit. The method used to process Solar Diameter Imager and Surface Mapper data of the PICARD distortion mode (Irbah et al. 2014), which is similar to the *SDO* calibration roll, is then applied for HMI image sequences.

The processing method is well detailed in Irbah et al. (2014) and the main steps are summarized here. The first step is to extract the solar shapes from the images in the sequence. The position of the inflection point of the limb-darkening function (LDF) for all azimuth angles is calculated for this purpose. LDF angular sampling of *SDO* images is good enough to detect photometric contaminations due to active regions (sunspots, faculae, etc.). The processing method that we used is based on a wavelet transform that preserves the LDF inflection point positions defining the solar shape, as bad or hard LDF filtering modifies its slope, which leads to inflection point shifts (Irbah et al. 1999). Nevertheless, active regions can still affect the mean solar shape that has been computed from all the ones in the sequence that have been previously re-phased in azimuth in order to remove the effects of both mispointing and optical distortion during averaging. These contaminations appear when solar active regions are localized very close to LDF inflection points. They are, however, easily detectable thanks to the roll procedure properties and then removed during processing.
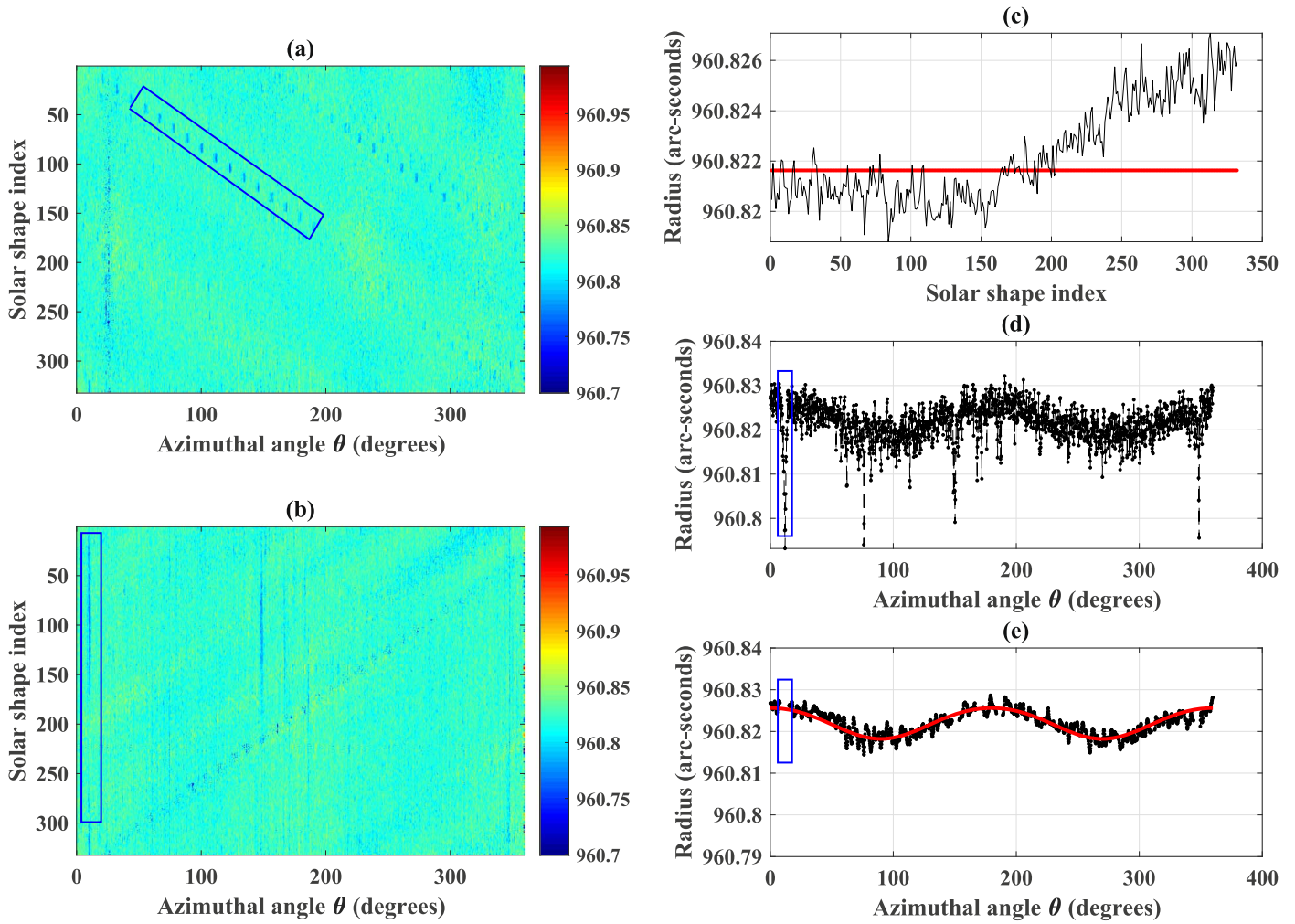
Figure 2. Roll sequence recorded on 2015 July 22, used to illustrate the processing method. (a) Azimuthal variations of solar radius obtained from images recorded during the roll. Each frame line coded in false colors corresponds to a solar shape calculated from one image. They are 332 images in this sequence, and the number of angular samples is 1800. Some active regions on the Sun (sunspots, faculae, etc.) as shown by their signature in the rectangle, existed that day and affect the solar shape. (b) Solar shapes are shifted so that they all have the western equator of the Sun at the zero azimuthal angle. Signatures of active regions affecting the shape are then spread out along frame columns while they are on oblique directions for CCD defaults. (c) A slight time drift of solar radius calculated from each shape (the black line) is observed during the roll. It is corrected by means of an iterative process (the red dashed line). (d) All shapes are averaged to compute the mean, where effects of active regions are clearly seen. (e) Active region effects on the solar shape are removed and then it is filtered to reduce the noise. The solar shape is fitted using low-order Legendre polynomials (the red curve) to estimate c_2 and c_4 distortion coefficients and, then the oblateness.

Indeed, rolling the spacecraft causes the solar image to rotate on the HMI charge-coupled device (CCD) camera. All CCD defaults remain in fixed positions in the frame while the solar features move with the spacecraft rotation. The roll sequence recorded on 2015 July 22 is taken to illustrate the main steps of the processing method. Azimuthal radius variations extracted from all of the images in the sequence are shown in Figure 2(a). They are coded in a false color frame, where each line is the azimuthal solar radius obtained from one image. Active regions on the extreme solar limb affect the radius at several azimuthal angles. Some effects are shown within the rectangle in Figure 2(a). These effects move in an oblique direction as the spacecraft rotates. Vertical features are also present, but these have clearly optical signatures as they remain fixed during roll operations. Figure 2(b) shows every azimuthal solar radius in the same reference frame; i.e., the West Equator is the origin of azimuthal angles for all lines. We notice that the solar active regions, surrounded by a rectangle in Figure 2(a), are now spread out along the same vertical direction. This is because they are quasi-fixed on the Sun's surface. The average radius of each line of the frame varies over time during the roll calibration (the black curve in Figure 2(c)). It is then corrected with an iterative process that computes the mean radius over the entire sequence (the red curve in Figure 2(c)). Finally, the solar shape, now free of both optical distortion and mispointing effects, is obtained by taking the radius mean value for each azimuthal angle (Figure 2(d)). The angular sampling is 0°.2. A part of the solar shape affected by active regions on the Sun's surface is shown in the region surrounded by a rectangle. Figure 2(e) plots the solar shape where solar active regions were removed and a wavelet transform filtering was applied to reduce the noise. The solar shape is then fitted using low-order Legendre polynomials (the red curve in Figure 2(e)). This polynomial fit, up to the fourth order, allows for the estimation of the quadrupole c_2 and the hexadecapole c_4 distortion coefficients. The solar oblateness is then given by
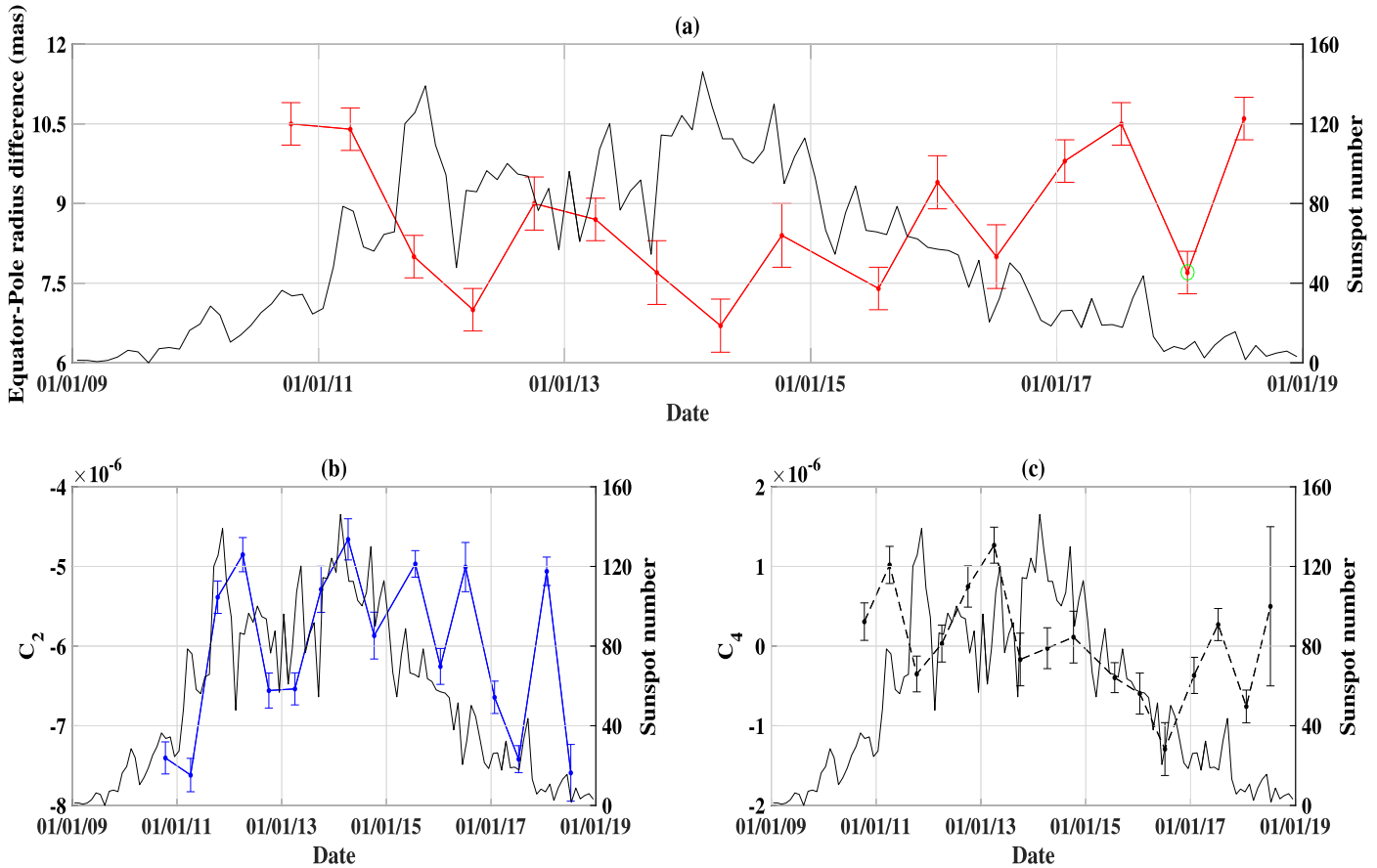
Figure 3. Fit model parameters of equator-pole radius difference obtained from HMI roll calibration images recorded during Cycle 24. (a) Time variations of solar oblateness (the red plot) are clearly in anti-phase with the sunspot number (the black line) taken as activity proxy. The value surrounded by green is thought to be underestimated due to poor determination and/or sudden solar events. The quadrupole variations C_2 (the blue dots) appear in phase with solar activity (b), whereas the hexadecapole C_4 (the black dots) has anti-symmetric variations relative to the time of solar activity maximum, where they are very small (c).

$\Delta R = -\frac{3}{2}c_2 - \frac{5}{8}c_4$, where ΔR is the pole-equator radius difference, or $\frac{\Delta R}{R} = -\frac{3}{2}C_2 - \frac{5}{8}C_4$ in the case of dimensionless C_2 and C_4; R is the mean solar radius.

3. Results and Discussion

Sixteen roll sequences, recorded between 2010 October and 2018 July, were analyzed according to the processing method presented in Section 2. The resulting average solar oblateness over the period 2010–2018 is 8.8 ± 0.8 mas, corresponding to a radius difference of 6.4 ± 0.6 km, which is in good agreement with measurements made over the past two decades (Egidi et al. 2006; Fivian et al. 2008; Rozelot et al. 2009; Irbah et al. 2014). They are also consistent with values predicted by helioseismology-based models (Armstrong & Kuhn 1999; Mecheri et al. 2004). This average value is, however, 1.6 mas higher than that reported by Kuhn et al. (2012) over the period of 2010–2012. In addition to the coherent values obtained for oblateness, variations in time of the solar shape are of particular importance in view of the scientific controversies surrounding historical measurements. The results obtained show not only that the solar oblateness exhibits variations, but also that these variations are in anti-phase with the sunspot number taken as proxy for the activity of the Sun (Figure 3(a)). This trend was suspected during the analysis of image sequences taken during the rising phase of Solar Cycle 24 (Meftah et al. 2016) and it is

confirmed by pursuing during almost the entire cycle. However, Kuhn et al. (2012) reported no change for the period 2010–2012 using the same *SDO* data. We calculated solar oblateness from the c_2 and c_4 values of their paper, and found a temporal trend that is similar to ours (see Figure 4). It should be noted that the roll calibration of 2018 January 24 gives a value of the solar shape that seems underestimated, in contrast to the emerging trend. The quadrupole C_2 exhibits variations that are clearly in phase with solar activity (Figure 3(b)). Indeed, a linear regression performed between C_2 values and sunspot number leads to $R^2 \approx 60\%$. Note also the yearly variations that seem to appear in the temporal evolution of C_2, in particular during the descent of the cycle of activity. More investigation is needed to find out if these variations are of solar origin or related to orbital correction residues.

Concerning the hexadecapole C_4, we notice that it has anti-symmetric variations relative to the time of solar activity maximum (Figure 3(c)). Indeed, C_4 exhibits variations during both the rising phase of Cycle 24, as already reported by Kuhn et al. (2012) for the period 2010–2012, and in the descent of the cycle (but of the opposite sign). This is clearly seen in Figure 5, where we fit C_2 and C_4 by sine functions over most of the cycle length. Rozelot et al. (2009), using C_2 and C_4 measurements of Emilio et al. (2007), interpreted these temporal variations of the oblateness by a change of the C_4 values that are insignificant when activity is important, but predominant when activity is
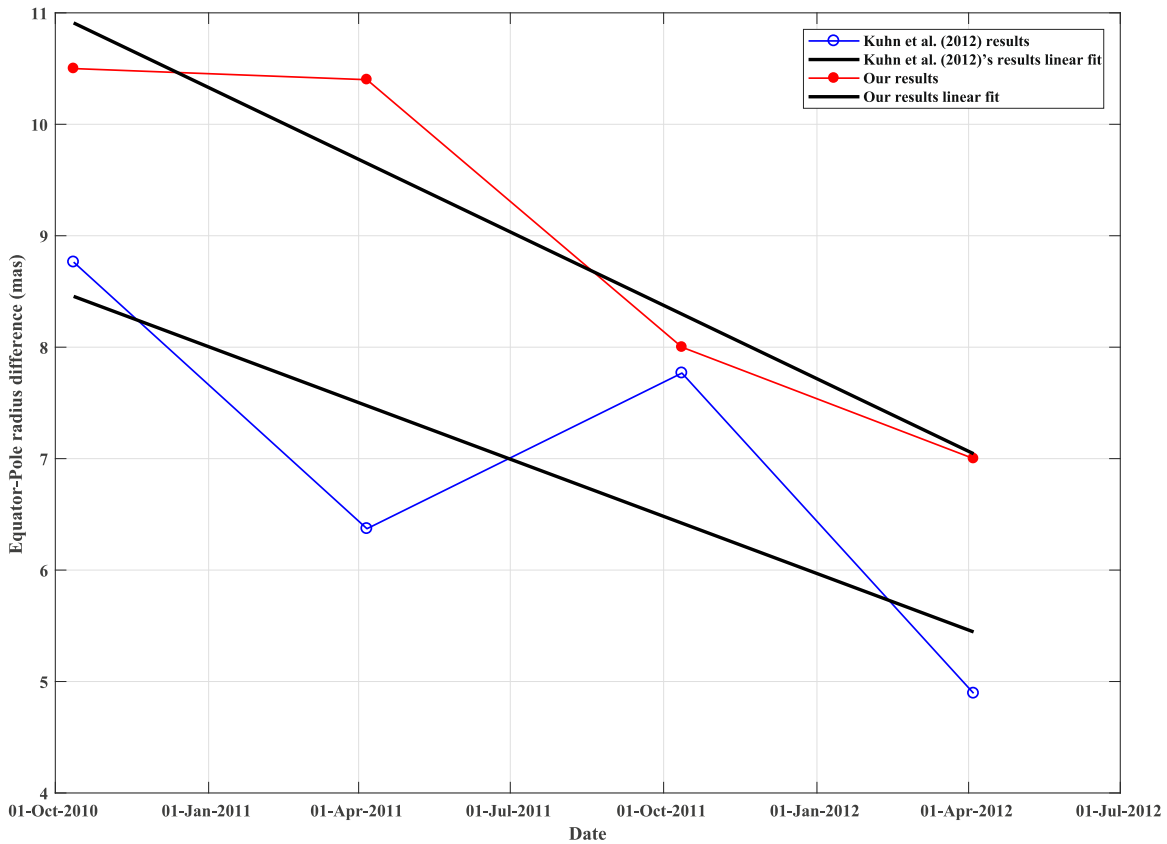
Figure 4. The same temporal trend of solar oblateness exists in the results of Kuhn et al. (2012), which are similar to ours.

low. They suggested that combining both should result in a variation of oblateness in phase with the solar cycle. We observe the same behavior of C_2 than Emilio et al. (2007) but in anti-phase. For C_4 we have low values at the extrema (minimum and maximum) of activity and the variations developing with changing activity (rise and fall). We indeed have a series of measurements that allows to understand the variation of C_4, whereas it is difficult to evidence a behavior with Emilio et al. (2007) as there are only two measurements (1997 and 2001), one of which has a large error (0.3 ± 2.5). They are, however, consistent with our measurements at high activity. We can see in Figure 3(c) that C_4 can vary rapidly in a short period of time, which could explain the difference with the Emilio et al. (2007) measurement obtained in low solar activity (1997).

We can conclude from our results that the solar shape is conditioned by both C_2 and C_4, where the former evolves in phase with solar activity, and the latter varies in phase quadrature with respect to the other. It is also worth comparing their action on the solar shape with that of a_2 and a_4, even asphericity coefficients deduced from helioseismology. A recent investigation using both MDI/*SOHO* and HMI/*SDO* helioseismic data over 21 yr revealed that during solar activity minimum the asphericity of the Sun is dominated by a_2 and a_4 splitting coefficients, while during solar activity maximum the a_2 coefficient, which primarily describes the solar oblateness, decreases considerably (Kosovichev & Rozelot 2018). This result indicates an anti-phase variation of the oblateness with solar activity during Cycle 24, which is in agreement with our results.

Linear regressions are performed on oblateness versus sunspot number considering all measurements performed during Cycle 24 (Figure 6(a)). The negative slope confirms the anti-phase of oblateness variations with the solar cycle. The linear regression R^2 is 61% when all HMI measurements are taken into account, and it increases to 77% (Figure 6(c)) when the poor estimated value of 2018 January 24 is removed (the value circled in green). The same approach is used for all oblateness measurements made during Cycle 23 with the Heliometer (Damiani et al. 2011), *RHESSI* (Fivian et al. 2008), and *SOHO*/MDI (Emilio et al. 2007). The linear regression shows a positive slope with $R^2 = 60\%$, reflecting oblateness variations in phase with solar activity during Cycle 23 (Figure 6(b)). The first measurement made in 2000 with the Heliometer, however, seems underestimated. This corresponds to the resumption of measurements after a 2 yr interruption. The linear regression R^2 increases to 79% when this value is removed (Figure 6(d)). Oblateness measurements performed on a balloon with the Solar Disk Sextant (SDS) in the descent of Cycle 22 are in anti-phase with the activity confirming the temporal oscillation of this solar parameter. Taken from the ground, measurements with the Heliometer made during the same period have a naturally limited precision and larger error bars, but properly overlap those of SDS (Figure 1), generating a higher confidence in their value. Both SDS and the Heliometer have the merit of allowing for advances in the knowledge of the temporal variability during a period when very little data was available. It is also worth noting Poor's analysis (1905) of earlier oblateness measurements made during Cycles 11 and 13, as well as that of Ambronn and Schur (1905) made during
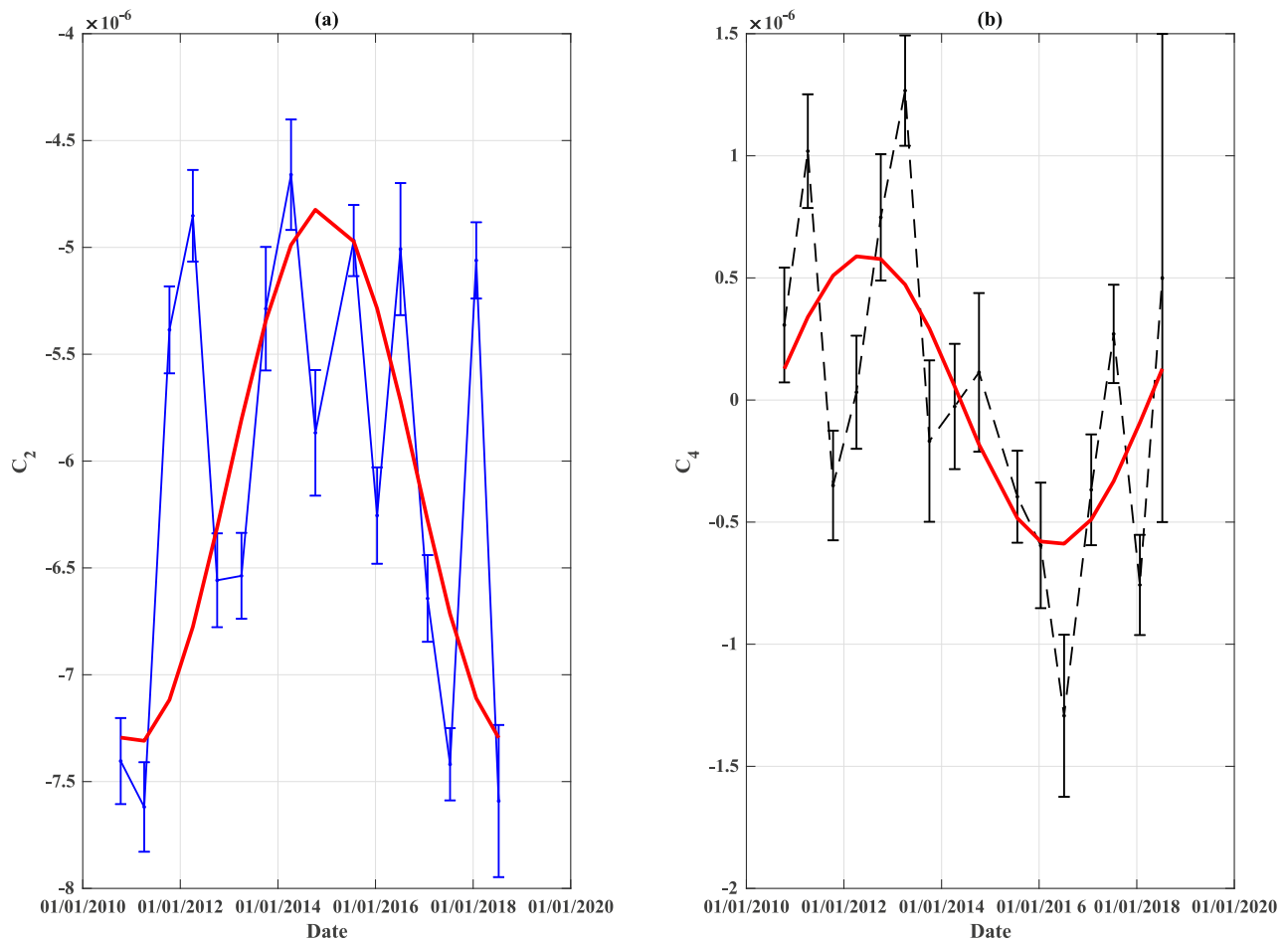
Figure 5. C_2 (a) and C_4 (b) temporal trends fitted with sine functions (the solid red lines) showing how they evolve during solar activity.

Cycles 11 and 12 (see Figure 1 in Damiani et al. 2011). Despite the limited precision of these historical measurements, variations (although very large) are clearly in phase with solar activity of Cycles 11 and 13. During Cycle 12, however, they are very similar to HMI variations observed around the maximum of solar activity; that is to say, in anti-phase. Accordingly, it is possible that the Sun initiates a physical process that results in a pulsation with a period of twice the 11 yr solar cycle. It has maximum swelling during odd cycles and vice versa for even ones; i.e., the solar shape oscillates like

the magnetic field having extreme values during its polarity inversion. It is therefore the time of the measurements, with respect to the temporal oscillation of solar oblateness, that largely explains the controversy surrounding past measurements reported in the literature. Why oblateness oscillates with the 22 yr magnetic cycle of the Sun is another challenge to model, which could probably be addressed by precise diagnostics of surface layer structure and dynamics. The complex structure of the leptocline, as defined in Reiter et al. (2015), is certainly a key to understanding this mechanism.
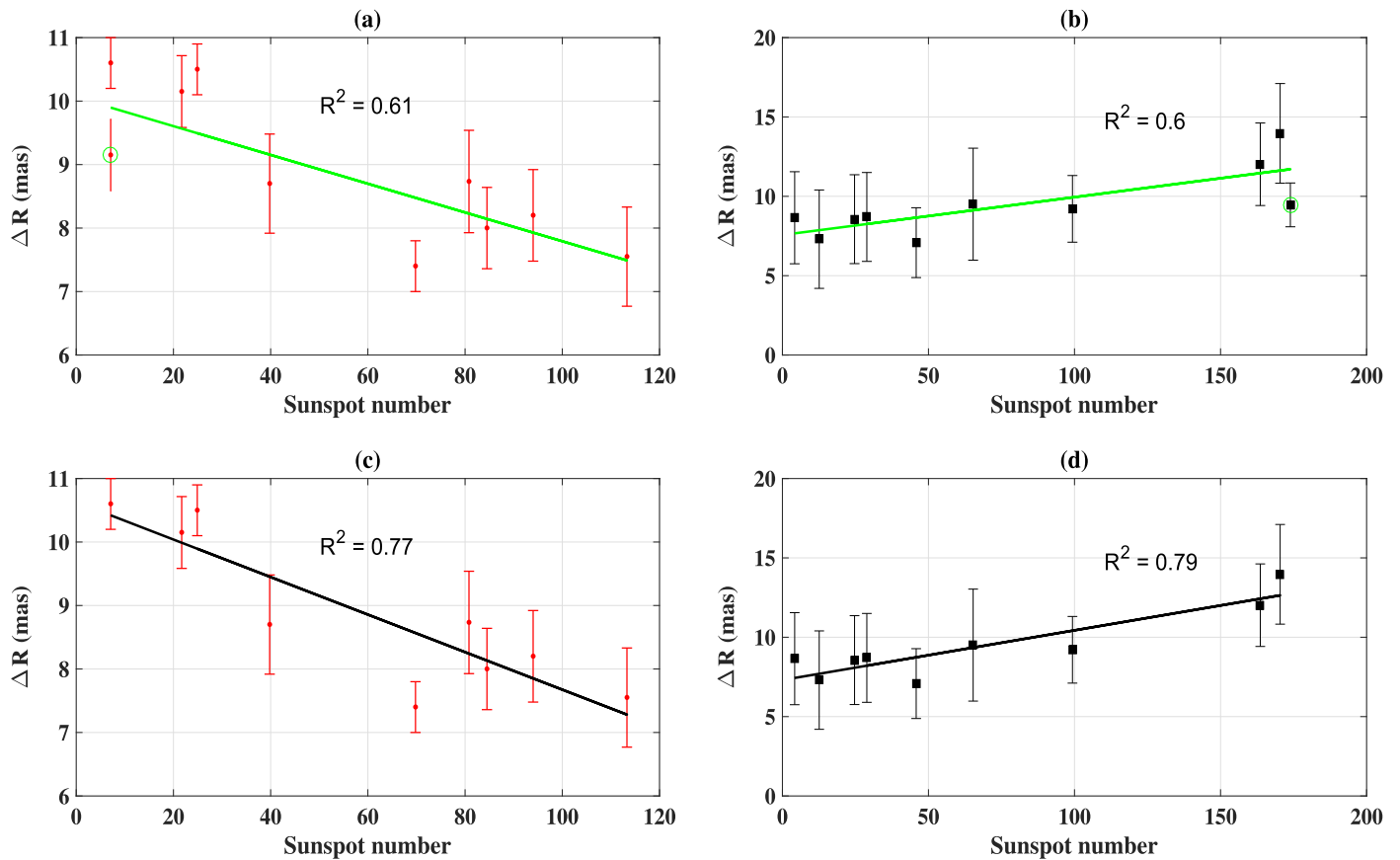
Figure 6. (a) All measurements of equator-pole radius difference made during Cycle 24 are plotted vs. sunspot number taken as proxy for solar activity. The linear regression performed on these two solar parameters is good giving $R^2 = 61\%$ (the green line). (c) The linear regression is better with $R^2 = 77\%$ (the black line) when the perturbed HMI measurement shown in Figure 3(a) by a dot surrounded with a green circle is not taken into account. The negative slope shows, as expected, that oblateness variations are in anti-phase with solar activity. (b) The same plot as in (a) when all measurements recorded during Cycle 23 are considered. The linear regression shows a positive slope with $R^2 = 60\%$, expressing that oblateness variations are in phase with solar activity during Cycle 23 (the green line). (d) A better linear regression is obtained with $R^2 = 79\%$ (the black line) when the supposed underestimated value recorded with the Heliometer in 2000 is not taken into account.

ORCID iDs

Abdanour Irbah ⓘ https://orcid.org/0000-0003-3265-3148

References

Antia, H. M., Chitre, S. M., & Gough, D. O. 2008, A&A, 477, 657
Antia, H. M., Chitre, S. M., & Thompson, M. J. 2000, A&A, 360, 335
Armstrong, J., & Kuhn, J. R. 1999, ApJ, 525, 533
Chapman, R. 2008, Sci, 322, 535
Damiani, C., Rozelot, J. P., Lefebvre, S., Kilcik, A., & Kosovichev, A. G. 2011, JASTP, 241
Dicke, R. H., & Goldenberg, H. M. 1974, ApJS, 241, 131
Dicke, R. H., Kuhn, J. R., & Libbrecht, K. G. 1987, ApJ, 318, 451
Egidi, R., Caccin, B., Sofia, S., et al. 2006, SoPh, 235, 410
Emilio, M., Bush, R. I., Kuhn, J., & Sherrer, P. 2007, ApJL, 660, L161
Fivian, M., Hudson, H., Lin, R., & Zahid, H. 2008, Sci, 322, 560
Goode, P. R., & Thompson, M. J. 1992, ApJ, 395, 307
Hill, H. A., & Stebbins, R. T. 1975, ApJ, 200, 471
Irbah, A., Bouzaria, M., Lakhal, L., Moussaoui, R., et al. 1999, SoPh, 185, 255
Irbah, A., Meftah, M., Hauchecorne, A., Djafer, D., et al. 2014, ApJ, 785, 89
Kosovichev, A. G., & Rozelot, J. P. 2018, JASTP, 176, 21
Kuhn, J. R., Bush, R., Emilio, E., & Scholl, I. F. 2012, Sci, 337, 1638
Le Verrier, U. J. 1859, Ann. Obs. Paris, 5, 1
Lefebvre, S., Rozelot, J. P., & Kosovichev, A. G. 2007, AdSpR, 40, 1000
Mecheri, R., Abdelatif, T., Irbah, A., Provost, J., & Berthomieu, G. 2004, SoPh, 222, 191
Meftah, M., Hauchecorne, A., Bush, R. I., & Irbah, A. 2016, AdSpR, 58, 1425
Newcomb, S. 1865, Fundamental Constants of Astronomy (Washington, DC: GPO)
Newcomb, S. 1895, BuAsI, 13, 26
Paterno, L., Sofia, S., & Di Mauro, M. P. 1996, A&A, 314, 940
Reiter, J., Rhodes, E. J., Jr., Kosovichev, A. G., Schou, J., et al. 2015, ApJ, 803, 92
Rozelot, J. P., & Damiani, C. 2011, EPJH, 36, 407
Rozelot, J. P., Damiani, C., & Pireaux, S. 2009, ApJ, 703, 1791
SILSO Data/Image 2018, Sunspot Number, WDC-SILSO, Royal Observatory of Belgium, Brussels
Sturrok, P. A., & Gilvarry, J. J. 1967, Natur, 216, 1280